Self-organizing maps for pattern recognition in design of alloys

Rajesh Jha[a], George S. Dulikravich[a], Nirupam Chakraborti[b], Min Fan[c], Justin Schwartz[c], Carl C. Koch[c], Marcelo J. Colaco[d], Carlo Poloni[e], and Igor N. Egorov[f]

[a]MAIDROC Laboratory, Department of Mechanical and Materials Engineering, Florida International University, Miami, FL, USA; [b]Indian Institute of Technology, Department of Metallurgical and Materials Engineering, Kharagpur, WB, India; [c]Materials Science and Engineering Department, North Carolina State University, Raleigh, NC, USA; [d]Mechanical Engineering Department, Federal University of Rio de Janeiro/COPPE, Rio de Janeiro, Brazil; [e]Dipartimento di Ingegneria e Architettura, University of Trieste, Trieste, Italy; [f]SIGMA Technology, Moscow, Russia

ABSTRACT

A combined experimental–computational methodology for accelerated design of AlNiCo-type permanent magnetic alloys is presented with the objective of simultaneously extremizing several magnetic properties. Chemical concentrations of eight alloying elements were initially generated using a quasi-random number generator so as to achieve a uniform distribution in the design variable space. It was followed by manufacture and experimental evaluation of these alloys using an identical thermo-magnetic protocol. These experimental data were used to develop meta-models capable of directly relating the chemical composition with desired macroscopic properties of the alloys. These properties were simultaneously optimized to predict chemical compositions that result in improvement of properties. These data were further utilized to discover various correlations within the experimental dataset by using several concepts of artificial intelligence. In this work, an unsupervised neural network known as self-organizing maps was used to discover various patterns reported in the literature. These maps were also used to screen the composition of the next set of alloys to be manufactured and tested in the next iterative cycle. Several of these Pareto-optimized predictions out-performed the initial batch of alloys. This approach helps significantly reducing the time and the number of alloys needed in the alloy development process.

Accepted 14 December 2016

KEYWORDS

Alloys; AlNiCo; design; magnets; metamodels; optimization; properties; SOM

Introduction

AlNiCo [1] are permanent magnetic alloys that have been widely used due to affordability, high-temperature stability, and excellent anticorrosion properties. A high magnetic energy density ($(BH)_{max}$) is desired as it helps to synthesize smaller magnets, while maintaining the superior magnetic properties. These magnets have high remanence (B_r) values that correspond to the amount of magnetic flux density left in the magnet after removal of the external magnetic field. AlNiCo magnets have lower coercivity (H_c) values and can be demagnetized in the presence of an external magnetic field. These alloys are first cast into complex shapes and thereafter magnetized in the production heat treatment stages.

A novel approach is presented here [2] for creating a work plan for efficiently using a set of computational tools for the design of alloy chemistry and multi-objective optimization [3–6] of desired macroscopic properties of various alloys [7–15]. This approach combines information from limited experimental databases with focus on stability of critical phases/structures [16, 17] while utilizing a number of numerical design optimization algorithms. These algorithms are based on several concepts from artificial intelligence including supervised and unsupervised machine learning algorithms [16, 17].

Materials and Methods

We selected eight alloying elements and set their concentration bounds after literature review (Table 1). Composition of the initial batch of 80 alloys was predicted by Sobol's quasi-random sequences generation algorithm [18]. These alloys were screened on the basis of phase equilibrium using Thermocalc [19] and Factsage [20]. A recent work from the developers of this software demonstrates the importance of phase transition diagrams [21] and we have also reported it in our recent works [2, 9, 14]. We performed a few *ab-initio*-based calculations to estimate the stable structures through open source database, Materials Project [22] that have been categorized on the basis of magnetic ordering and stability. Both *ab-initio* calculations and phase transformation diagrams through CALPHAD approach are effective for predicting properties of alloys with up to four alloying elements [21, 22].

These 80 initial alloys were then manufactured and tested for: magnetic energy density ($(BH)_{max}$), magnetic coercivity (H_c), magnetic remanence (B_r), saturation magnetization (M_s), remanence magnetization (M_r), ($(BH)_{max}$)/mass, magnetic permeability (μ), intrinsic coercivity field ($_jH_c$). The experimental data were used to build eight-dimensional response surfaces linking alloy composition to desired properties. Several meta-models were developed using various

CONTACT George S. Dulikravich dulikrav@fiu.edu Florida International University, MAIDROC Laboratory, Department of Mechanical and Materials Engineering, Miami, FL 33174, USA.

Table 1. Concentration bounds for alloying elements in AlNiCo type alloys [2].

	Variable bounds (weight percent)		
Alloying elements	1–85	86–143	144–180
Cobalt (Co)	24–40	24–38	22.8–39.9
Nickel (Ni)	13–15	13–15	12.35–15.75
Aluminum (Al)	7–9	7–12	6.65–12.6
Titanium (Ti)	0.1–8	4–11	3.8–11.55
Hafnium (Hf)	0.1–8	0.1–3	0.095–3.15
Copper (Cu)	0–6	0–3	0–4.5
Niobium (Nb)	0–2	0–1	0–1.5
Iron (Fe)		Balance to 100%	

approaches, tested on various accuracy measures and the most accurate one was chosen for further study [5]. Meta-models that were selected were then used to simultaneously maximize the properties listed above, while minimizing cost of the raw materials and alloy mass density. We actually used several distinct multi-objective optimization algorithms [3–6]. Due to limitations of some of the optimizers, it was decided to Pareto-optimize chemical compositions of alloys for the three optimized properties ($(BH)_{max}$, B_r, and H_c) and then use these compositions to predict the other seven properties. From this Pareto set, we selected a few alloys for further manufacture and testing. Candidate alloys were screened on the basis of phase stability, along with several statistical measures [2, 5, 14, 19–22]. Alloys that satisfied the above analysis were selected for manufacture and testing in the next cycle. The entire process was terminated after a total of 180 alloys (initial random chemistry of 80 alloys plus 100 alloys generated in 10 computational design/experimental verification cycles) were created. Unsupervised learning algorithms such as principal component analysis (PCA) [5], hierarchical clustering analysis (HCA), [5] and self-organizing maps (SOM) [23] were used to discover various patterns within the dataset.

Results and Discussion

Figure 1 shows the second quadrant of the B–H curve with all the 180 alloys plotted on it. Alloys are marked according to the method that was used to generate that composition.

It can be seen that alloy 124 predicted by this design methodology is the best alloy according to the three optimized properties. Figure 2 shows the distribution of all 10 properties and 8 alloying elements that will be helpful to determine the alloys (or a group of alloys) that perform best for most of the properties.

In order to minimize the number of alloys compositions that need to be manufactured and experimentally tested, we also used a classification technique that is based upon an unsupervised neural network, popularly known as SOMs or self-organizing feature maps [23] proposed by Teuvo Kohonen in the 1980s. SOM implements a term competitive learning along with a neighborhood function to preserve the topological properties of the dataset [23]. This makes SOM a perfect tool to visualize high-dimensional datasets in lower dimensions, usually two to three, while preserving the topology for determining various correlations within the dataset [24]. SOMs can be considered as a nonlinear generalization of PCA [5, 25]. Recent studies demonstrate the advantage of using SOM over PCA [23, 26]. Most importantly, SOMs have

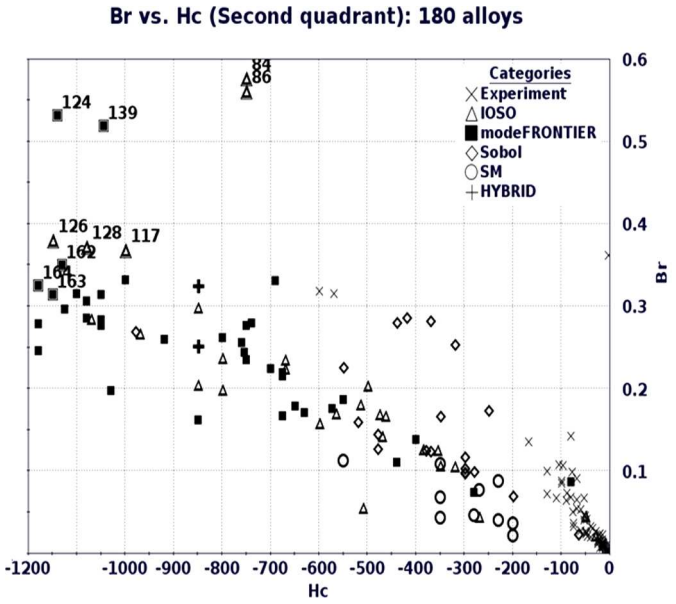

Figure 1. Scatter plot of 180 alloys on the second quadrant of B–H curve [2].

been successfully used for feature extraction of scarce datasets (sample size of about 40), whereas conventional neural networks require large training sets [27, 28]. In this work, we used a commercial optimization package mode FRONTIER for SOM analysis [5] which uses the following steps.

1. Learning cycle: For our dataset, we used Batch SOM, where the learning cycle is updated after all the sample data are presented to the network.
2. Setup training parameters: In the following text, key setting parameters are introduced, that were adjusted during the analysis.
   - X-dimension and Y-dimension: It is an integer positive value and it represents the dimension of a component of the Kohonen map. The default value was set at 8 since there were 8 alloying elements.
   - Map units: It is an integer positive value and it represents the dimension of the Kohonen map, which in this case was 64. The default value was set in a way that the ratio between X-dimension and Y-dimension is equal to the ratio between the first two principal eigenvalues of the dataset.
   - Initialization type: We used linear initialization where the initial map is obtained by using a linear combination of Kohonen map dimension and the two principal eigenvalues of the dataset.
   - Random seed: This is an integer number, usually used for sequence repeatability. That is, if two SOMs are generated with the same seed, they will return identical maps. For a more random distribution, seed value can be set to 0. In this case, the map is automatically seeded with a value that is based on the current time, which is never identical, and hence, there is less chance of sequence repetition.

Apart from these, there exist a few more parameters, namely, initial rough radius, final rough radius, rough phase radius, initial fine tuning radius, final fine tuning radius, and fine tuning phase length. All of these parameters have an

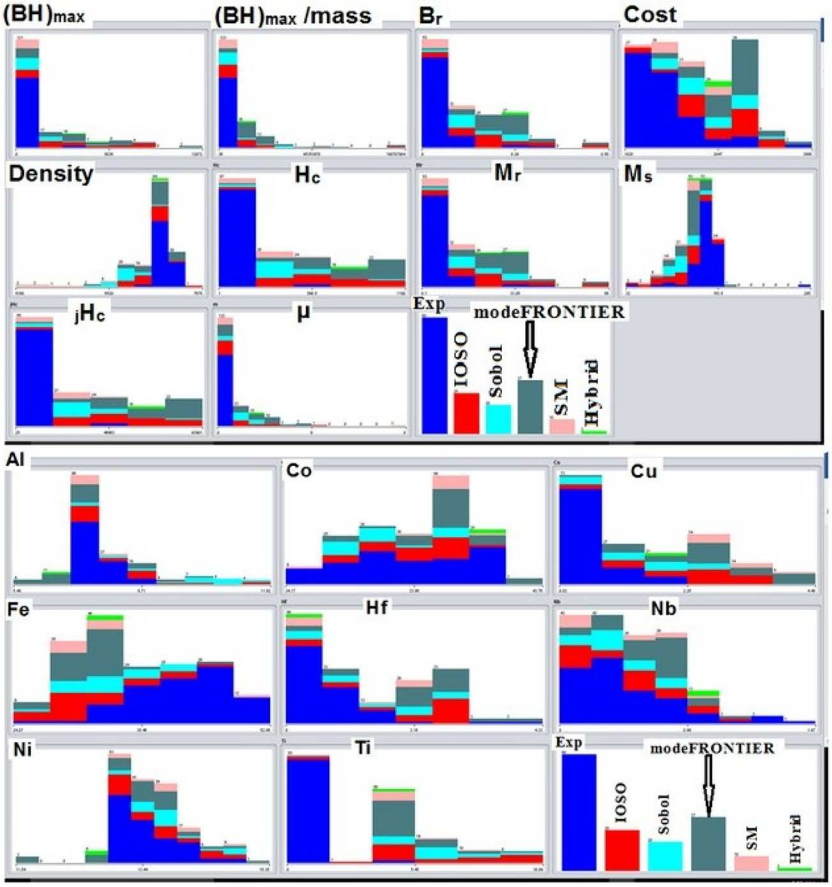

Figure 2. Distribution of properties and elements of the magnet for different classes (or approaches).

integer positive value which needs to be fine tuned during the analysis so as to minimize the topological error that was found to be 0.043 in the present analysis [5]. Readers are advised to follow the cited references for better understanding of these parameters.

Our purpose of using SOM maps can be listed as follows:

- Find correlations between various variables and properties that can be supported from the literature.
- Classify the dataset in various clusters and identify the units/clusters with candidate alloys with a set of superior properties.
- This way predicts the chemical composition of alloys for superior properties.
- This approach was used as an additional screening tool for selecting a set of alloys to be manufactured in the next alloy design cycle.

Here, the experimentally verified alloys were added to Pareto-optimized predictions. Thereafter, the maps were created followed by clustering analysis through HCA over SOM maps. Pareto-optimized alloys that belonged to the units with superior properties (or alloys that were in the adjacent units) were given preference as these alloys are both Pareto-optimized and statistically verified and expected to perform similar to the previous best. This will be explained in more detail in the following sections.

As mentioned before, SOM charts are divided into hexagonal units. In this case, the number of units was set at 64. SOM D-matrix chart shows the average distance between a unit and its six nearest neighboring units. For each unit, mean values of the distance from its six nearest neighbors are calculated and are used to represent that unit. Peaks of units can be used to detect clusters in the input dataset. SOM D-matrix is to be used in conjunction with SOM P-matrix chart for identifying the clusters within the dataset (Fig. 3).

SOM P-matrix chart is a representation of the probability density of input data and can be used to detect probability density-based cluster structures. In this chart (Fig. 3), we can see for each cell the (relative) number of designs for which that cell and its six neighbors are the best matching unit. Here, peaks of dense zones of the input space are separated by valleys of sparse ones. SOM P-matrix chart must be used with D-matrix chart for identifying clusters. In D-matrix, all 180 alloys were placed on the chart to show the way these alloys were distributed in 2D space.

In the P-matrix chart, we decided to identify the units that consist mostly of alloys that are included in top 10 candidate alloys ranked on the basis of $(BH)_{max}$ values. This way, we identified three units, 48, 56, and 57, as the units that need to be examined for finding correlations in the dataset. Additionally, it must be noted that these three units are adjacent to each other. This further proves the efficacy of using these maps to discover correlations within a high-dimensional dataset in reduced 2D space. One can see that there is a square present in the center of each unit. The size of the square depends on the number of alloys that are included in this unit.

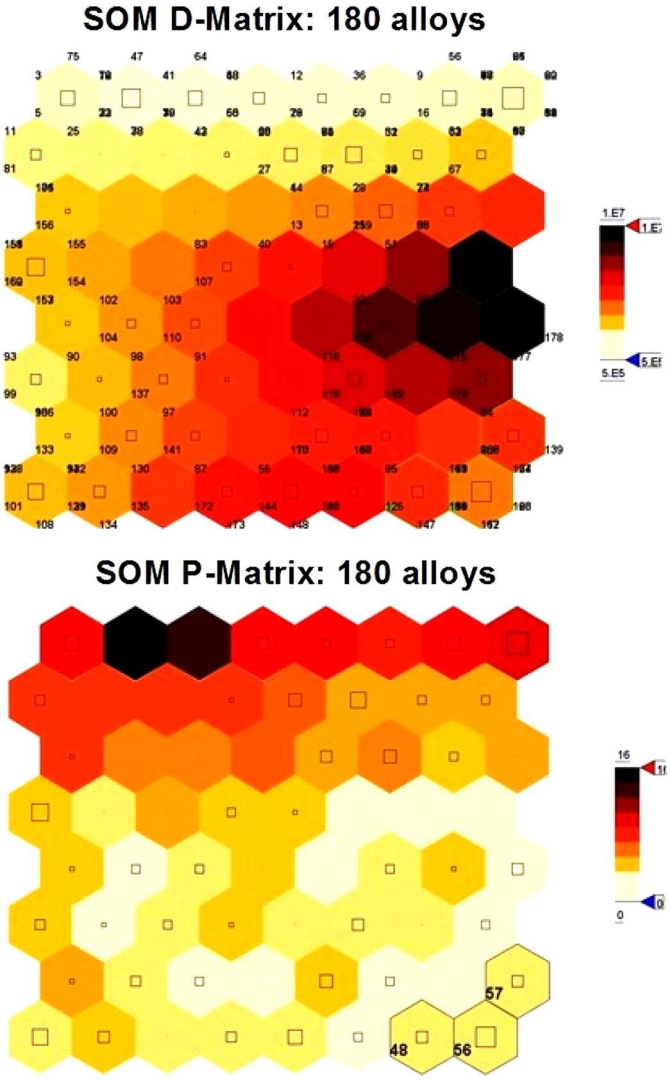

Figure 3. SOM D-matrix and SOM P-matrix chart for 180 alloys.

It can be seen that in a few units, the square is reduced to a point. These units can be removed from the chart and will not affect the analysis. The candidate alloys that were included in units 48, 56, and 57 were

- Unit 48 consists of alloys 95, 125, 147, 165.
- Unit 56 consists of alloys 111, 114, 117, 126, 127, 128, 143, 161, 162, 163, 164, 166, 169, 180.
- Unit 57 consists of alloys 84, 86, 124, 139.

All of these alloys are Pareto-optimized predictions apart from alloy 95 which was predicted by Sobol's algorithm [18] and is the best performer in the 4th design cycle. Thus, this method can be used as an alternative method to screen alloys for manufacture as alloys in adjacent units have superior properties and have a better chance to mimic the properties of previous best alloys.

Component chart (Fig. 4) shows the distribution of different components, variables, and properties on the SOM hexagonal grid where similar component maps are placed in adjacent positions. Hence, it is easy to spot correlations between the properties and variables. Figure 4 shows the component plots for all of the variables and properties in a 2D plot.

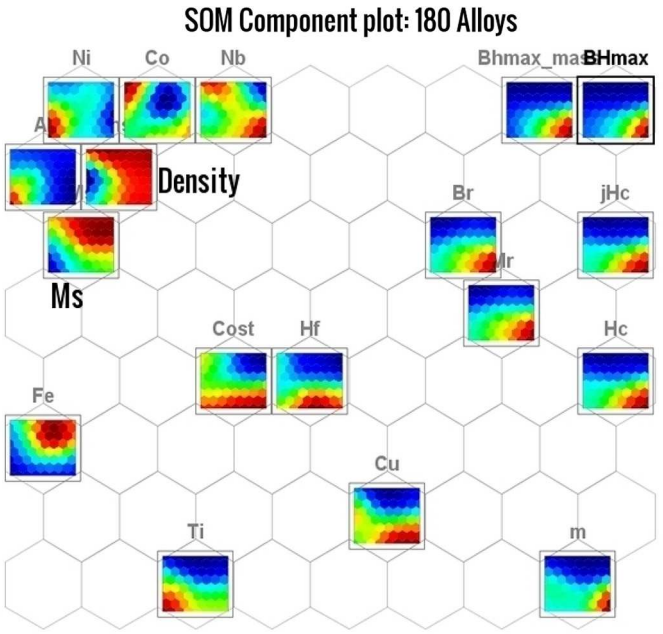

Figure 4. Component plot for 180 alloys.

From Fig. 4, one can observe that $(BH)_{max}$ and $(BH)_{max}$/mass are in adjacent units. Thus, SOM maps were able to detect strong correlations between these two properties. Similarly, B_r and M_r are adjacent to each other and it points toward a possible correlation between these two properties. Also, H_c is inverse of $_jH_c$, and it can also be seen that these two units are close to each other. This information will be helpful in reducing the number of properties to be optimized, thus, reducing the complexity of the problem.

For better understanding of the system, our focus will be on the three units identified before, that is, alloys contained in units 48, 56, and 57. Table 2 shows the SOM prediction for properties of candidate alloys and alloying elements that are part of these units.

Table 2 and Fig. 5 can be used to conclude the following.

1. $(BH)_{max}$: Units 56 and 57 have the highest $(BH)_{max}$ values. Best alloys are placed in the adjacent units. This means that the topology of the dataset is preserved.

Table 2. SOM component analysis results for properties and alloying elements for units 48, 56, and 57.

Properties/elements	Unit 48	Unit 56	Unit 57
$(BH)_{max}$	5042	6046	6116
H_c	944.76	996	957.82
B_r	0.296	0.323	0.331
M_s	122.79	124.17	126.57
M_r	33.03	36	37.02
$(BH)_{max}$/Mass	5.16E7	5.74E7	5.92E7
μ	1.12E-4	1.41E-4	1.46E-4
Cost	3035.45	3039	2974
$_jH_c$	75173	79257	76220
Density	7151	7152	7142
Al	7.336	7.243	7.236
Co	35.803	36.281	36.366
Cu	2.856	2.826	2.62
Fe	32.207	32.050	32.659
Hf	2.471	2.351	2.119
Nb	0.757	0.80	0.801
Ni	13.49	13.44	13.395
Ti	5.07	4.99	4.807

2. Units 48, 56, and 57 contain the best alloys that can be classified on the basis of B_r, H_c, M_r, M_s, μ, $(BH)_{max}$/mass, and $_jH_c$.
3. Three properties were optimized (maximized), namely, $(BH)_{max}$, B_r, H_c, but SOM analysis shows that M_r, M_s, μ, $(BH)_{max}$/mass, and $_jH_c$ were also maximized as a result of it.
4. M_s: These units contain alloys with average M_s values.
5. Density: These units contain alloys with density that is lower than average values.
6. Cost: These units contain the best alloys for several properties but are comparatively the most expensive ones.

From Fig. 6, we can observe that optimized iron content is slightly higher than the lowest value reported in the figure. Optimized cobalt composition is about the average value reported in the figure. Optimized aluminum content is about the lowest value reported in the figure. Optimized nickel content varies in a very narrow range that is slightly higher than the lower bound, but less than the average value reported in Fig. 6. From Table 2, one can observe that the SOM predictions for alloying elements of alloys contained in units 48, 56, and 57 are within the composition range reported for commercial alloys.

Figure 7 shows the component plot of titanium. It can be seen that units 48, 56, and 57 have titanium content that varies in a small range which is about the average value shown in the figure. The reported titanium contents of commercial alloys are also in this range. Thus, SOM plots proved to be helpful in optimizing the titanium content of alloys.

Figure 7 also shows the component plot of copper. It can be seen that units 48 and 56 have similar copper contents that are about the highest value reported in the dataset, while unit 57 has slightly lower copper content. It must be noted that similar trends were observed in the component plots of properties for H_c and $_jH_c$. From literature, it is known that copper precipitates out of α_2 phase and these precipitates were observed on the Cu–Ni-rich bridges between adjacent α_1 phases [29]. H_c is an extrinsic property and it depends on the microstructure variation at the nanometer level. Thus, lower H_c for unit 57 can be attributed to comparatively lower copper content of alloys in unit 57. The reported copper content of commercial alloys is also in this range. Thus, SOM plots proved to be helpful in optimizing the copper content of alloys.

Figure 7 further shows the component plot of hafnium. It can be seen that units 48, 56, and 57 have hafnium content that varies in a small range which is between the average value and is slightly less than the highest value shown in the figure. Hafnium has not been used in commercial AlNiCo alloys. In our work, we observed traces of hafnium precipitates on the Cu–Ni bridges between adjacent α_1 phases [29]. This topic needs further investigation. A detailed analysis of the effect of Hf on the formation of Cu–Ni-rich bridges will be helpful to understand the phenomenon of phase separation for improved magnetic properties. Figure 7 also shows the component plot of niobium. It can be seen that units 48, 56, and 57 have similar niobium content which is about the highest values reported in the figure. SOM predicted niobium content is within the reported niobium content of commercial alloys.

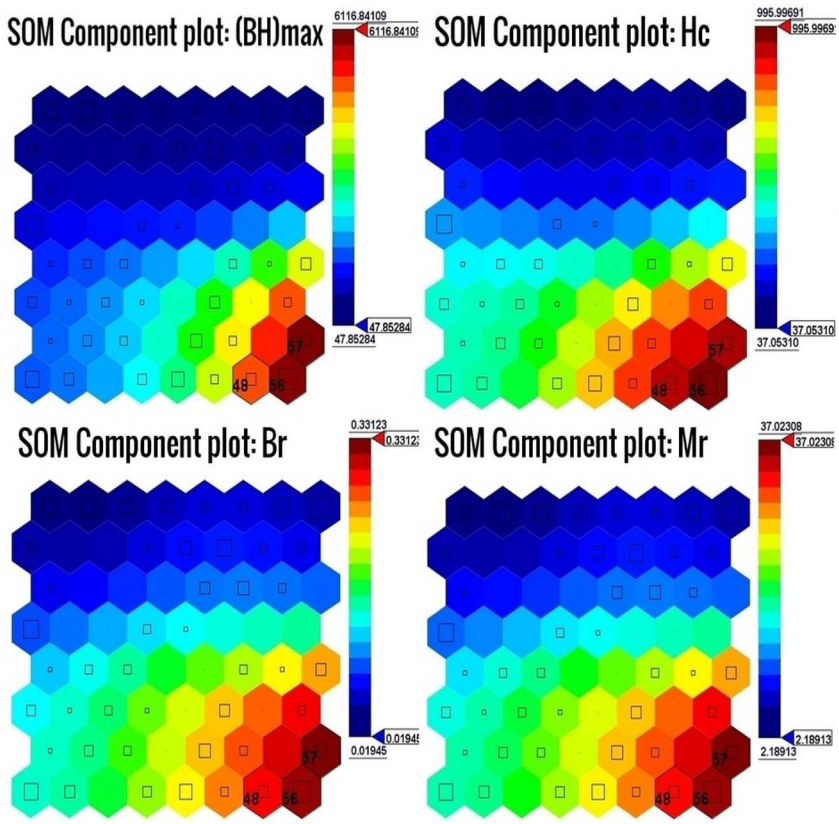

Figure 5. SOM component plot for $(BH)_{max}$, B_r, H_c, and M_r.

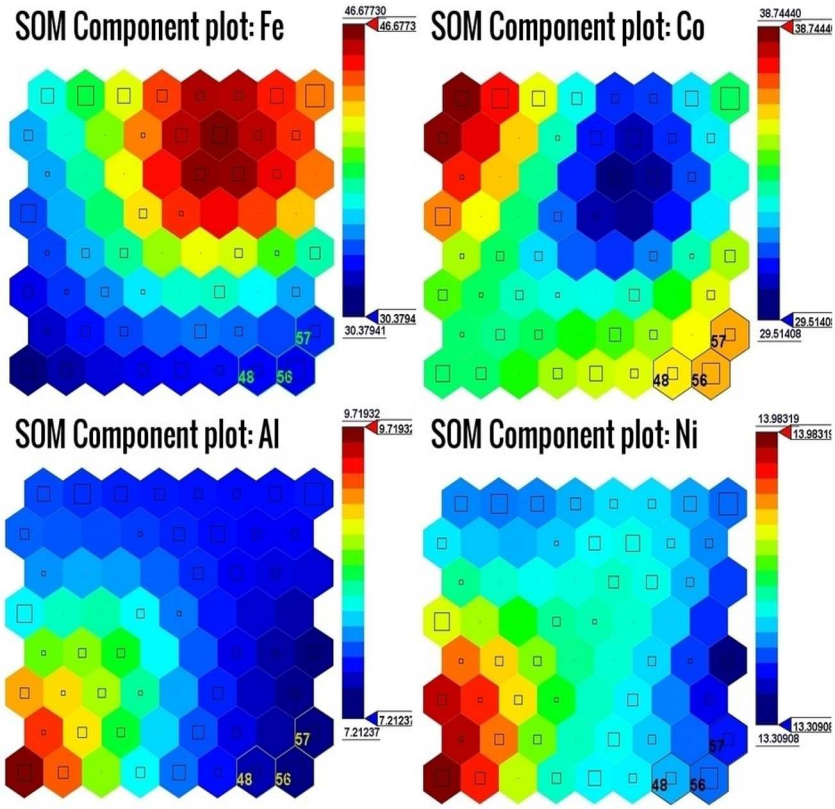

Figure 6. SOM component plot for iron, cobalt, aluminum, and nickel.

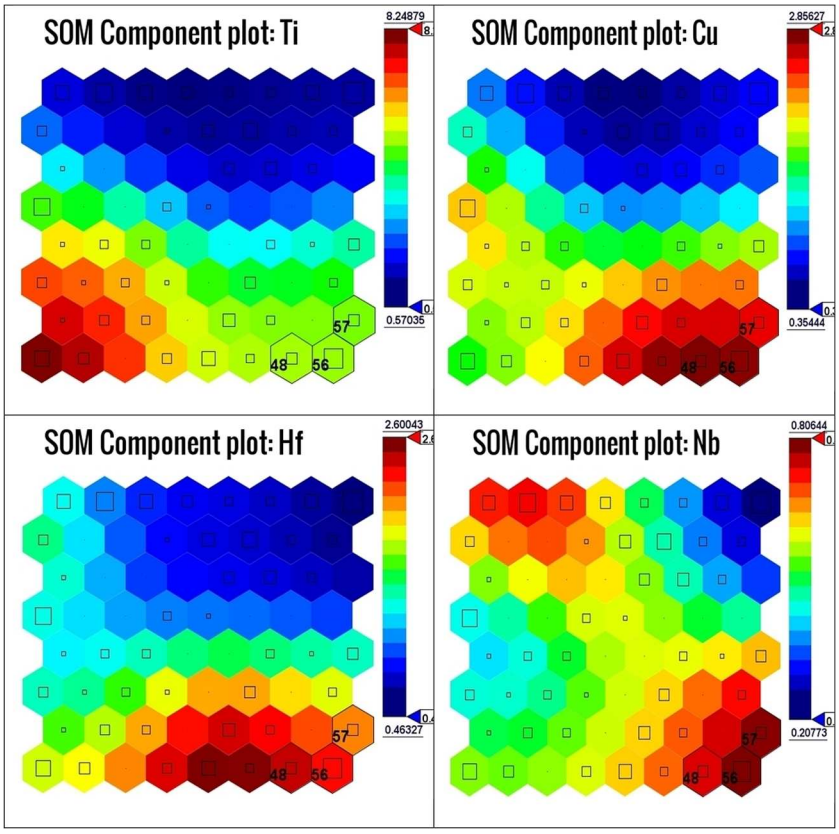

Figure 7. SOM component plot for titanium, copper, hafnium, and niobium.

Conclusions

In this work, we presented a novel approach to design chemistry of a class of AlNiCo alloys using a set of computational tools that were routinely checked for improvements through experimentation. Such an approach can prove to be useful for designing new alloys and their accelerated implementation. Key components of the contribution of this work can be listed as

1. Efficient use of a random number generator to predict the initial set of compositions with the help of information about the system reported in the open literature.
2. Efficient use of phase stability and transformation diagrams for screening alloys prior to manufacture.
3. Use of *ab-initio* calculations to predict magnetic properties of structures that need to be stabilized for improved properties.
4. Use of response surface methods to develop metamodels for linking chemical composition to macroscopic properties of alloys.
5. Multi-objective optimization of targeted properties to predict the composition of new alloys for improvement in their properties.
6. Use of phase transformation diagrams, and several statistical methods to screen candidate alloys to be manufactured in the next cycle.
7. Use of SOM as a tool to predict the composition of alloys that perform well for a set of properties.
8. A guideline for effective use of SOM maps for screening alloys for improved properties.
9. $(BH)_{max}$, B_r, and H_c were maximized together, while SOM analysis shows that for the optimized alloys that are part of units 48, 56, and 57, seven properties were maximized as a result of optimization, namely, $(BH)_{max}$, B_r, H_c, M_r, μ, $(BH)_{max}$/mass, and ${}_jH_c$. These alloys have average M_s and density while most of these alloys were expensive. This demonstrates the efficacy of meta-model-based prediction and multi-objective optimization followed by data analysis by use of unsupervised learning methods in alloy design.

Acknowledgments

This work was partially funded by the US Air Force Office of Scientific Research (grant number FA9550-12-1-0440) monitored by Dr. Ali Sayir. The lead author is also thankful for the Dissertation Year Fellowship provided by the University Graduate School, Florida International University. The views and conclusions contained herein are those of the authors and should not be interpreted as necessarily representing the official policies or endorsements, either expressed or implied, of the US Air Force Office of Scientific Research or the US Government. The US Government is authorized to reproduce and distribute reprints for government purposes notwithstanding any copyright notation thereon.

References

[1] Zhou, L.; Miller, M.; Lu, P.; Ke, L.; Skomski, R.; Dillon, H.; Xing, Q.; Palasyuk, A.; McCartney, M.; Smith, D.; Constantinides, S.; McCallum, R.; Anderson, I.; Antropov, V.; Kramer, M. Architecture and magnetism of AlNiCo. *Acta Materialia* **2014**, *74*, 224–233.

[2] Jha, R. Combined Computational-Experimental Design of High-Temperature, High-Intensity Permanent Magnetic Alloys with Minimal Addition of Rare-Earth Elements, Ph.D. thesis, Manuscript # 3734, https://digitalcommons.fiu.edu/etd/2621/.

[3] Egorov, I.N. Indirect Optimization method on the basis of self-organization, Curtin University of Technology, Perth, Australia. *Optimization Techniques and Applications (ICOTA'98)* **1998**, *2*, 683–691.

[4] Deb, K. *Multi-Objective Optimization using Evolutionary Algorithms*; John Wiley and Sons: Chichester, UK, 2001.

[5] ESTECO: modeFRONTIER, http://www.esteco.com/modefrontier (accessed on January 3, 2015), 2015.

[6] Dulikravich, G.S.; Colaco, M.J. Hybrid optimization algorithms and hybrid response surfaces. In *Advances in Evolutionary and Deterministic Methods for Design, Optimization and Control in Engineering and Sciences*; D. Greiner, B. Galvn, J. Periaux, N. Gauger, K. Giannakoglou, G. Winter, Eds.; Chapter 2, Springer Verlag: Heidelberg, 2015; 19–47.

[7] Egorov-Yegorov, I.N.; Dulikravich, G.S. Chemical composition design of superalloys for maximum stress, temperature, and time-to-rupture using self-adapting response surface optimization. *Materials and Manufacturing Processes* **2005**, *20*, 569–590.

[8] Dulikravich, G.S.; Egorov, I.N. Inverse design of alloys' chemistry for specified thermo-mechanical properties by using multi-objective optimization, Chapter 8. In *Computational Methods for Applied Inverse Problems*, Inverse and Ill-Posed Problems Series 56; Y.F. Wang, A.G. Yagola, C.C. Yang, Eds.; Walter De Gruyter and Higher Education Press: China, 12 September 2012; 197–219, ISBN: 978–3-11–025905-6

[9] Jha, R.; Pettersson, F.; Dulikravich, G.S.; Saxen, H.; Chakraborti, N. Evolutionary design of nickel-based superalloys using data-driven genetic algorithms and related strategies. *Materials and Manufacturing Processes* **2015**, *30* (4), 488–510.

[10] Jha, R.; Dulikravich, G.S.; Colaco, M.J.; Egorov, I.N.; Poloni, C.; Chakraborti, N.; Fan, M.; Schwartz, J.; Koch, C.C. Magnetic alloys design using multi-objective optimization. In MS&T15-Materials Science and Technology 2015 Conference, Columbus, Ohio, October 4–8, 2015.

[11] Jha, R.; Dulikravich, G.S.; Chakraborti, N.; Fan, M.; Schwartz, J.; Koch, C.C.; Colaço, M.J.; Poloni, C.; Egorov, I.N. Algorithms for multi-objective design optimization of hard magnetic alloys using experimental data. In ICMM4-International Conference on Material Modeling, Berkeley, CA, May 27–29, 2015.

[12] Jha, R.; Dulikravich, G.S.; Colaco, M.J.; Fan, M.; Schwartz, J.; Koch, C.C. Magnetic alloys design using multi-objective optimization. In ACEX2015–9th International Conference on Advanced Computational Engineering and Experimenting, Munich, Germany, June 29–July 2, 2015.

[13] Jha, R.; Dulikravich, G.S.; Chakraborti, N.; Fan, M.; Schwartz, J.; Koch, C.C.; Colaço, M.J.; Poloni, C.; Egorov, I.N. Algorithms for design optimization of chemistry of hard magnetic alloys using experimental data. *Journal of Alloys and Compounds* **2016**, *682*, 454–467, doi:10.1016/j.jallcom.2016.04.218.

[14] Jha, R.; Dulikravich, G.S.; Colaco, M.J.; Fan, M.; Schwartz, J.; Koch, C.C. Magnetic alloys design using multi-objective optimization. In *Properties and Characterization of Modern Materials*, Advanced Structured Materials series, Vol. 33; A. Oechsner, L.M. da Silva, H. Altenbac, Eds.; Springer: Germany, 2016; 261–284, 978–981-10–1601-1 doi:10.1007/978-981-10-1602-8_22.

[15] Giri, B.K.; Hakanen, J.; Miettinen, K.; Chakraborti, N. Genetic programming through bi-objective genetic algorithms with a study of a simulated moving bed process involving multiple objectives. *Applied Soft Computing Journal* **2013**, *13* (5), 2613–2623.

[16] Mueller, T.; Kusne, A.; Ramprasad, R. Machine learning in materials science: Recent progress and emerging applications. *Reviews in Computational Chemistry* **2016**, *29*, 186–273.

[17] Kusne, A.G.; Gao, T.; Mehta, A.; Ke, L.;Nguyen, M.C.; Ho, K.M.; Antropov, V.; Wang, C.Z.; Kramer, M.J.; Long, C.; Takeuchi, I. On-the-fly machine-learning for high-throughput experiments; search for rare-earth-free permanent magnets. Scientific Reports 4 published online (15 September 2014) article no. 6367, doi:10.1038/srep06367.

[18] Sobol, I.M. Distribution of points in a cube and approximate evaluation of integrals. *USSR Computational Mathematics and Mathematical Physics*, **1967**, *7*, 86–112.
[19] Thermocalc: http://www.thermocalc.com/solutions/by-application/alloy-development (accessed on January 3, 2015), 2015.
[20] Factsage, http://www.factsage.com (accessed on January 3, 2015), 2015.
[21] Bale, C.W.; Bélisle, E.; Chartrand, P.; Decterov, S.A.; Eriksson, G.; Gheribi, A.E.; Hack, K.; Jung, I.-H.; Kang, Y.-B.; Melançon, J.; Pelton, A.D.; Petersen, S.; Robelin, C.; Sangster, J.; Spencer, P.; Van Ende, M-A. FactSage thermochemical software and databases, 2010–2016. *CALPHAD: Computer Coupling of Phase Diagrams and Thermochemistry* **2016**, *54*, 35–53.
[22] Jain, A.; Ong, S.P.; Hautier, G.; Chen, W.; Richards, W.D.; Dacek, S.; Cholia, S.; Gunter, D.; Skinner, D.; Ceder, G.; Persson, K.A. The materials project: a materials genome approach to accelerating materials innovation. *APL Materials* **2013**, *1* (1), 011002.
[23] Self-organizing Map, https://en.wikipedia.org/wiki/Self-organizing_map (accessed on August 20, 2016).
[24] Pena, M.; Barbakh, W.; Fyfe, C. Topology-preserving mappings for data visualisation, principal manifolds for data visualization and dimension reduction. In *Lecture notes in computational science and engineering*, Vol. 58; A.N. Gorban, B. Kégl, D.C. Wunsch, A.Y. Zinovyev, Eds.; 2008; 131–150, ISBN: 978–3-540–73749-0 (Print) 978–3-540–73750-6 (Online).
[25] Yin, H. Learning nonlinear principal manifolds by self-organising maps, principal manifolds for data visualization and dimension reduction. In *Lecture notes in computational science and engineering*, Vol. 58; A.N. Gorban, B. Kégl, D. C. Wunsch, A.Y. Zinovyev, Eds.;, 2008; 68–95, ISBN: 978–3-540–73749-0 (Print) 978–3-540–73750-6 (Online).
[26] Liu, Y.; Weisberg, R.H.; Mooers, C.N.K. Performance evaluation of the self-organizing map for feature extraction. *Journal of Geophysical Research* **2006**, *111*, C05018, doi:10.1029/2005JC003117.
[27] Pettersson, F.; Chakraborti, N.; Saxen, H. A genetic algorithms based multi-objective neural net applied to noisy blast furnace data. *Applied Soft Computing* **2007**, *7* (1), 387–397.
[28] Krasznai, E.Á.; Boda, P.; Csercsa, A.; Ficsór, M.; Várbíró, G. Use of self-organizing maps in modelling the distribution patterns of gammarids (Crustacea: Amphipoda). *Ecological Informatics* **2016**, *31*, 39–48.
[29] Fan, M.; Liu, Y.; Jha, R.; Dulikravich, G.S.; Schwartz, J.; Koch, C. Effect of Cu-Ni-rich bridges on the microstructure and magnetic properties of alnico alloys. *IEEE Transactions on Magnetism* **2016** August; *52* (8), 1–10.